Modeling and Control Design for a Turboelectric Single Aisle Aircraft Propulsion System

Joseph W. Connolly,* Jeffryes W. Chapman,† Erik J. Stalcup,‡ Keith R. Hunker§
NASA Glenn Research Center, Cleveland, OH 44135, USA

Amy K. Chicatelli,¶ George L. Thomas‖
Vantage Partners LLC, Brook Park, OH 44142, USA

A nonlinear dynamic model with full flight envelope controller is developed for the propulsion system of a partially turboelectric single-aisle aircraft. The propulsion system model consists of two turbofan engines with a large percentage of power extraction, feeding an electric tail fan for boundary layer ingestion. The dynamic model is compared against an existing steady state design model. An electrical system model using a simple power flow approach is integrated into existing modeling tools used for dynamic simulation of the turbomachinery of the vehicle. In addition to the simple power flow model of the electrical system, a more detailed model is used for comparison at a key vehicle transient flight condition. The controller is a gain scheduled proportional-integral type that is examined throughout the flight envelope for performance metrics such as rise time and operability margins. Potential improvements in efficiency for the vehicle are explored by adjusting the power split between the energy used for thrust by the turbofans and that extracted to supply power to the tail fan. Finally, an operability study of the vehicle is conducted using a 900 nautical mile mission profile for a nominal vehicle configuration, a deteriorated propulsion system at the end of its operating life, and an optimized power schedule with improved efficiency.

I. Nomenclature

EGT	=	exhaust gas temperature
f	=	frequency
F_N	=	net thrust
i	=	current
I	=	spool inertia
j	=	waypoint index
K_i	=	integral gain
K_p	=	proportional gain
N_f	=	fan rotational speed
N_H	=	high spool rotational speed
N_L	=	low spool rotational speed
P	=	power
P_s3	=	high pressure compressor static exit pressure
P_T	=	total pressure
Q	=	reactive power
RU	=	ratio unit ($\frac{W_f}{P_s3}$)
T_T	=	total temperature
V	=	voltage

*Aerospace Engineer, Intelligent Control and Autonomy Branch, 21000 Brookpark Rd., 77-1, AIAA Senior Member
†Aerospace Engineer, Propulsion Systems Analysis Branch, 21000 Brookpark Rd., AIAA Member
‡Aerospace Engineer, Thermal Systems and Transport Processes Branch,21000 Brookpark Rd.
§Electrical Engineer, Thermal Energy Conversion Branch, 21000 Brookpark Rd., 301-1
¶Aerospace Engineer, 3000 Aerospace Parkway VPL-3, AIAA Senior Member
‖Aerospace Engineer, 3000 Aerospace Parkway VPL-3, AIAA Member

W = flow rate
Y = admittance
Δ = change in parameter
δ = voltage phase angle
η = efficiency
γ = admittance angle
π = ratio of the circumference of a circle to its diameter
τ = torque

Subscripts

c = corrected parameter
cmd = command
G = generator
i, j = node number
L = load
m = motor
n = shaft index
s = static condition

II. Introduction

The National Aeronautics and Space Administration (NASA) is exploring advanced technologies to significantly reduce the emissions from future aircraft[1]. The dominant source of emissions in the aviation market today is from aircraft larger than the regional transport class[2]. While NASA is developing technologies for more electric aircraft at every size class[3, 4], the focus of this paper is on the larger class vehicle where there is greater potential for emissions reduction given the current aviation market. One of the largest advantages of electric aircraft is the ability to move power to various parts of the aircraft more efficiently than by using mechanical components[5–7]. The current challenge for electric aircraft is the power density of energy storage devices not comparing favorably to the energy density of jet fuel. To meet the objective of emissions reductions for larger aircraft in the foreseeable future, a combination of distributed electric power and turbofan engines providing power generation is expected.

Fig. 1 Single aisle turboelectric concept aircraft with aft boundary layer ingestion.

Distributed propulsion systems for large aircraft are commonly designed to use gas turbine engines that drive electric generators in order to provide enough total power to meet the requirements of distributed fans[8–12]. In partially turboelectric systems, such as the Single-aisle Turboelectric AiRCraft - Aft Boundary Layer (STARC-ABL)[13], the turbine engine must produce a local thrust in addition to supplying power to an electrical generator for distributed thrust using a tail fan. Even for the lightly distributed STARC-ABL shown in Fig 1, the percentage of shaft power converted to electricity in the generator can exceed 25%. Since the goal of power redistribution is to reduce overall energy use and fuel burn, it will be important to verify that the engine itself does not incur a significant efficiency penalty or performance degradation while maintaining lifecycle operability expectations.

This paper investigates control and operability concerns for the STARC-ABL initial design concept to ensure viability across an expected mission profile. The focus is on the development of a nonlinear dynamic propulsion system model capable of capturing the dominant system level dynamics between the traditional turbofan engine, aft tail fan, and the interconnecting electrical power system of the STARC-ABL concept. Furthermore, a baseline propulsion system controller is developed along with supporting control schedules for the power extraction throughout the flight envelope. The propulsion system model is integrated with a simple steady state electrical power system model. That is, the power

system is assumed to have instantaneous dynamics compared to the propulsion system. Thus, the power system is modeled as an algebraic system, not a dynamic one. In addition, propulsion system data are fed through a separate, more complex dynamic power system model as a check on the steady state power flow model used for overall system studies. The simple model enables rapid propulsion system control trade studies throughout the flight envelope, but without a detailed electrical system model. A more complex dynamic power system model is able to capture the electrical system controller at key operating conditions for detailed investigations of system interactions. The propulsion control systems will play a critical role to ensure operability requirements of the partially distributed systems are met by modifying traditional control schedules.

The rest of the paper is structured starting with an overview of the single aisle turboelectric concept vehicle, followed by a description of the propulsion system model and its control system. Next, a discussion is provided on the modeling variations for the electrical system. The results section includes a linear propulsion system study throughout the flight envelope, showing the controlled response of the integrated STARC-ABL concept model at a key flight condition, an exploration of potential improvements to efficiency, and an operability study of a 900 nautical mile (nmi) mission profile. Finally, conclusions are provided.

III. Single Aisle Turboelectric Aircraft Concept Overview

The STARC-ABL concept utilizes a simple turboelectric propulsion architecture from an electrical power distribution perspective. This concept aircraft can be viewed as a bridge from current designs used in industry to the ultimate goal of improved aerodynamic efficiency through highly distributed propulsion. The aircraft size class considered by this study accommodates 150 passengers with a cruise speed of 0.78 Mach and a maximum range of 3,500 nmi. Only a partial distribution of power to the tail fan was used in the STARC-ABL concept shown in Fig. 1. The twin geared turbofans still provide a significant amount of thrust, 80% during takeoff and 55% at the top of climb (TOC) condition[13]. The turboelectric architecture enables the decoupling of the power producing elements from the thrust producing elements, which provides the potential for distribution of the propulsors. This concept allows for the implementation of a turboelectric architecture without the added complexity of a fully distributed propulsion system, which would include numerous additional electrical system components, energy storage devices, motors, and fans. It should be noted that the initial STARC-ABL design does not include a battery, but there is an expectation that a small amount of energy storage may be required for load leveling between the turbofan and tail fan.

While thermal issues are a large technical challenge for these vehicle concepts, it will not be addressed in the current study. The thermal issue is partially due to the simple fact that excess heat is not being exhausted to the atmosphere as is done in a typical turbofan engine, but also because the heat from the power system has a lower gradient than heat generated from the engine, which makes mitigation strategies more difficult.

The turbofan engine for this study needs to provide both thrust and electrical power, a concept schematic of the turbofan engine is shown in Fig. 2(a). In most current turbofan engine configurations, power for cabin needs is extracted off of the high pressure spool (HS). This is done in part due to the need for the engine to be able to restart in the event of an inflight shutdown. The HS has a lower inertia, thus less power is required to increase the rotational speed of the spool in the event of a needed restart when compared to the low speed spool (LS). Due to the relatively low level of electrical power needed for cabin purposes, generators are currently connected to the HS and extract a low percentage of the over all HS power. By comparison, the power required for distributed propulsors is much higher. Therefore, in order to accommodate distributed power concepts, power needs to be extracted from the LS, because that is where turbofan engines generate the vast majority of their power. A generator is shown in Fig. 2(a) connected to the LS. The power obtained from the two generators, corresponding to the two turbofan engines employed in the concept aircraft, is then distributed to independent tail motors. These motors power the tail fan shown in Fig. 2(b).

Each of the turbofan engines has an independent electrical bus, generator, and motor interconnected to accommodate the potential loss of a single engine. The tail fan is positioned such that it can reenergize the flow in the boundary layer to improve the overall aerodynamic performance of the vehicle and improve overall fuel efficiency. Trade studies are ongoing to investigate the expected efficiency improvement reported in the initial studies[13]. While the tail fan could potentially be driven by a turbofan engine, this turboelectric concept enables technology development and demonstration required for the more distributed propulsion system. Weight increases and efficiency losses would be expected for a more distributed propulsion system when implemented mechanically. In the current configuration, the electrical power requirements are driven by the tail fan, which amounts to 2.6 Mega Watt (MW). Consequently, the generators are each required to provide 1.44 MW, which provides a total with some excess to account for the losses in the power system. Each turbofan engine is therefore required to provide power in excess of 1.44 MW.

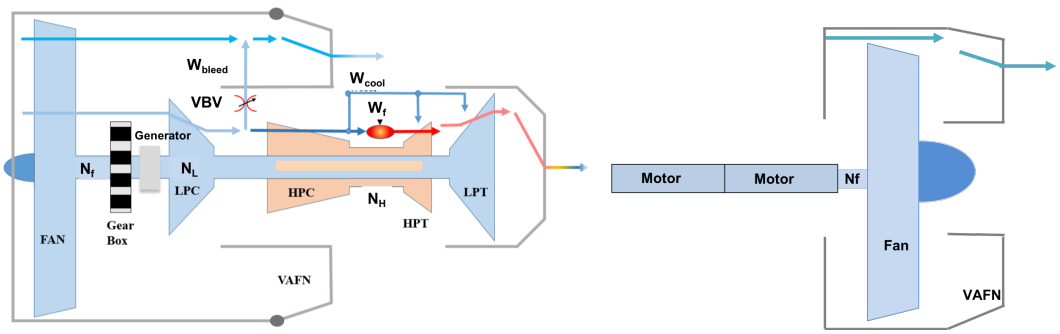

(a) Turbofan. (b) Aft tail fan.

Fig. 2 (a) Conceptual turbofan configuration with generator pulling power from the low speed spool. (b) Conceptual electric motor driven fan located at the tip of the aircraft tail cone.

IV. Modeling and Control System Architecture

Nonlinear dynamic models of the turbomachinery and electrical power systems have been developed that are representative of the STARC-ABL concept. Two versions of each of the models have been developed. On the turbomachinery side, a steady state design model was first developed using the Numerical Propulsion System Simulation (NPSS)[14] that includes both of the turbofans, tail fan, and a simple power system model. In addition, a turbomachinery dynamic model was developed using the Toolbox for the Modeling and Analysis of Thermodynamic Systems (T-MATS)[15]. T-MATS is an open-source toolbox written and developed for use in MATLAB/Simulink. A simple power flow model of the electrical system was developed with a direct goal of easily interfacing with T-MATS. The purpose of this model is to facilitate control studies of the propulsion system with representative electrical component models. A more detailed electrical system model that includes the high frequency electrical dynamics and controller was also developed using MATLAB/Simulink Simscape Power Systems™. The focus here will be on the T-MATS turbomachinery model and the MATLAB/Simulink power flow model to enable broader propulsion system control trade studies.

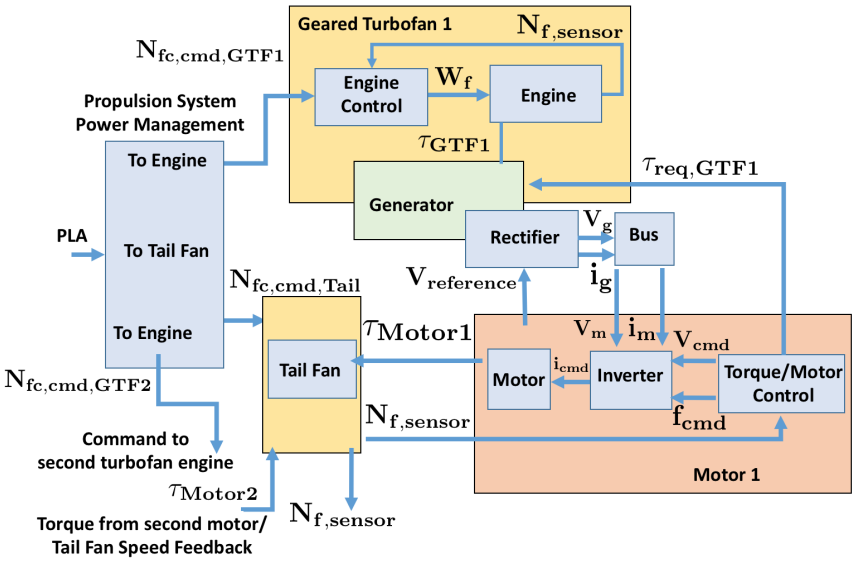

Fig. 3 Propulsion system control schematic with electrical power systems.

A general propulsion-electrical system control approach is shown in Fig. 3. The philosophy behind this approach is that an electric-enabled aircraft propulsion system should be operated nearly identically to the propulsion system in a traditional aircraft. Specifically, a pilot manipulates the power lever angle (PLA) to bring about a transient

response of thrust from the system that would be comparable to that of a traditional propulsion system. A pilot under normal operation would only need to adjust a single PLA setting, with the option to send individual commands to the geared turbofan and tail fan in fault scenarios. A significant change for this system is that the PLA sends not just an $N_{fc,cmd,GTF1}$ (fan rotational speed) command that correlates with thrust to the turbofans, but an additional $N_{fc,cmd,Tail}$ command to the tail fan. The schematic in Fig. 3 only shows a single geared turbofan engine (GTF1), but the actual system has a second identical geared turbofan engine (GTF2). Each geared turbofan has a generator that extracts power from the low-speed spool shaft that supplies power to a specific motor on a common tail fan spool. This creates two independent electrical system strings, one for each geared turbofan. In each electrical system string an alternating current (AC) from the generator travels through a rectifier to transport the power over a direct current (DC) bus operating at 1,000 volts. The motor controller, indicated with the "torque/motor control" block, commands the inverter to deliver the commanded current (i_{cmd}), at the appropriate voltage (V_{cmd}) and frequency f_{cmd}, to generate the desired torque (τ_{Motor1}). The desired torque is determined by the tail fan speed controller, which regulates the tail fan speed to the setpoint value provided by the propulsion system power management controller. The torque/motor control also provides information to the generator so that the corresponding amount of required torque ($\tau_{req,GTF}$) from each geared turbofan can be extracted. For nominal operation, the required amount of power needed by the tail fan is extracted evenly from each of the turbofans. In the event of a fault in one of the turbofans, the tail fan should still be able to receive a minimum of 50% of its required power. Detailed studies will be needed to understand the optimal power split between the tail fan and turbofan in a fault scenario at various phases of flight. The modeling and controls schemes for the turbomachinery and electrical system will be discussed in greater detail in the following subsections.

A. Propulsion System Modeling

The primary components for the turbomachinery T-MATS model are shown in Fig. 2. Generic compressor blocks are used for the fan, low pressure compressor (LPC), and high pressure compressor (HPC) components, while generic turbine blocks are used for the high pressure turbine and low pressure turbine (LPT). Individual turbomachinery components are assumed to be zero dimensional, where the component-level gas dynamics are not modeled. Internal component calculations contain a combination of physics based and empirical models. Algebraic relations and component maps are used to generate component or system steady state solutions at specific operating points. For example, compressor efficiency (η), corrected mass flow (W_c), and pressure ratio (PR) are determined from the compressor map as functions of corrected shaft speed (N_c) and R-line, where R-line is an uniquely defined line on the compressor map. A generic illustration of a compressive component performance map is shown in Fig. 4. This figure shows the expected turbomachinery trends as additional power is extracted from the geared turbofan. The operating line of the HPC of the engine will move closer to the surge line with a shift in corrected speed. Conversely, the operating line of the LPC on a generic performance map will shift downwards to provide a lower overall pressure ratio and more stall margin. Finally, the fan performance characteristics typically follows that of the LPC.

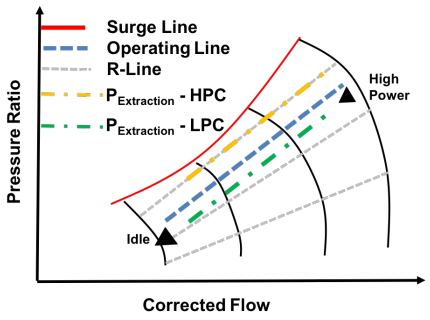

Fig. 4 Generic compressive component map showing the operating line (dashed blue), surge (red), speed lines (black) and R-lines (dashed grey), movement of the HPC operating line due to power extraction (yellow), and movement of the LPC operating line due to power extraction (green).

The generic performance maps used in the T-MATS model are scaled to be representative of the STARC-ABL concept based on the output data of the steady state design NPSS model[13], used as a truth model. The first step in the process for developing the dynamic turbofan model is matching a steady state T-MATS model against the NPSS output data at 726 distinct operating points across the flight envelope. The distinct operating conditions for altitude and Mach are shown in Fig. 5, where at each point a sweep of distinct points in the PLA operating range is conducted. A red box is drawn around the cruise points, a key condition of interest that is explored later for possible efficiency gains through alteration of the vehicle power split.

At each operating condition, the T-MATS turbomachinery components are compared to the NPSS model using a steady state simulation where the direct fuel flow, W_f, variable bleed valve (VBV), and variable area fan nozzle (VAFN), are set to the known NPSS condition. This is done for every component with the exception of the tail fan VAFN, where the area change is reduced across the range of flight conditions to be more aligned with expected actuator capabilities.

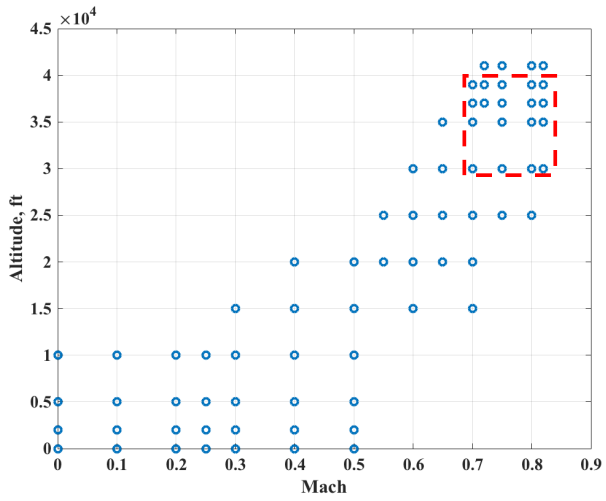

Fig. 5 Flight envelope operating conditions.

The NPSS model comparison is done with the T-MATS model configured as both a new engine and an end of life engine to get expected performance across the lifecycle of the vehicle. The T-MATS variables of total pressure (P_T), total temperature (T_T), and mass flow rate (W) are shown as average percent differences from the NPSS model for the core and bypass stations of the engine in Table 1. The difference between the two models is generally less than half a percent across the flow stations for the new engine. The end of life engine has the greatest variation on the mass flow. One important feature that is illustrated in the deteriorated engine is that the core of the engine is impacted more than the bypass. This could imply that as the turbomachinery components degrade it may be beneficial to generate more thrust from the tail fan, as it will degrade similarly to the bypass stream of the turbofan. Additional details of the comparison between NPSS and T-MATS can be found in the appendix.

Table 1 T-MATS geared turbofan % difference from NPSS

	Average Core Stations			Average Bypass Stations		
	W	P_T	T_T	W	P_T	T_T
New	0.33	0.26	0.16	0.58	0.24	0.09
End of Life	6.51	2.91	3.44	2.53	0.68	0.29

The T-MATS model was then modified to include the dynamics of the shaft inertias. The individual turbomachinery components are connected such that the flow from the inlet (ambient conditions) is connected to the fan block which is followed by a splitter block that splits the flow into core and bypass paths. The fan is connected to the LS through the T-MATS Gear Box block. The fan, LPC, and LPT torques are summed to comprise the input to the LS. In addition to a conventional turbofan engine, a generator block is included on the LS. This generator represents the electrical component of the turbofan that enables distributed propulsion. The generator torque is summed as part of the LS torque balancing. The HPC, HPT, and a cabin power generator torque are summed to comprise the input torque to the HS. The unbalanced torques on the shafts provide the dominant dynamic response of the turbofan engine, where the shaft accelerations ($\dot{N}_n$) are calculated as shown in Eq. 1.

$$\dot{N}_n = \frac{\sum(\tau_{i,turbomachinery} + \tau_{i,generator})}{2\pi I} \tag{1}$$

The rotor accelerations and the flow errors from each component, including the nozzle, are inputs to the Jacobian calculator block. The Jacobian calculator determines the independent variables, which are the R-line for compressors, pressure ratio for turbines, a total flow for the input to the inlet, the splitter ratio, and the updated rotor speeds. The iterative solver makes use of the Newton-Raphson method to step a plant toward a solution. Each of the two turbofans in the propulsion system is modeled as described above. The propulsion system also includes an electrically driven, ducted fan, that ingests the boundary layer. This fan is modeled as a single shaft, with a modified inlet model that accounts for the effects of boundary layer ingestion on the inlet total pressure, as well as a fan component, and a variable area nozzle.

From the dynamic T-MATS model, a piece-wise linear model (PWLM) was developed to enable the controller design. T-MATS handles the linearization of the nonlinear model through the calculated Jacobian using a small perturbation method at each operating condition. These models are then linked together to approximate the nonlinear model through a linear interpolation scheme[16]. The linear model and steady state model compare essentially equivalently to the NPSS model at all of the operating conditions.

B. Propulsion System Controller

A baseline control architecture for a turbofan engine equipped with a full authority digital engine control is shown in Fig. 6. Turbofan engine controllers are designed to regulate a measurable variable such as corrected fan shaft speed (N_{fc}), which is correlated with thrust[17]. This is done since there is no on-board sensor for thrust. The main interface between the pilot and the control system is the PLA or throttle, which is used by the controller logic to set a required N_{fc} command. The measured N_{fc} is subtracted from the command set point to create an error signal that goes to the controller to determine a fuel flow rate (W_f). Protection logic limits the commanded fuel flow rate to provide safe operation of the engine[18–22]. The feedback controller and limiters are designed as gain scheduled proportional-integral (PI) type with integrator windup protection. In addition to the main controller, open loop schedules for the VBV, VAFN, and power extraction are included. Output data from the STARC-ABL NPSS model were used to develop the scheduled control parameters based on the corrected fan speed, Mach number, and altitude. The resulting power extraction schedule is shown in Fig. 7(a). Correspondingly, the electrical power required to drive the tail fan is shown in Fig. 7(b). For the current configuration, the maximum power required is 2.6 MW. As a result, the two generators are required to provide up to 1.44 MW each, which includes an additional amount to account for losses within the system. The power control schedule was determined by matching the turbofan to the design fan percent corrected speed with constraints on maximum turbine inlet temperature.

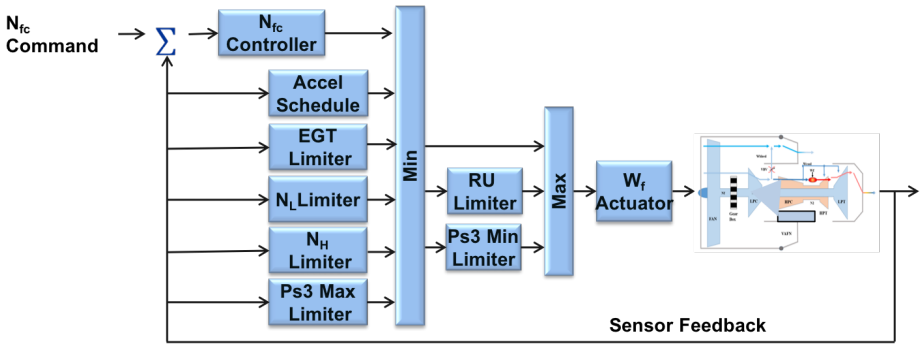

Fig. 6 Baseline full authority digital controller diagram with a min/max protection logic.

For safety and operability, protection logic is used to regulate excessive transients and other operating limits that could lead to stall or other engine failures, as shown in Fig. 6. This is done by monitoring sensed parameters for the engine shafts acceleration, combustor pressure, maximum low speed spool (N_L) and high speed spool (N_H), and the ratio unit (RU), which is W_f over compressor discharge static pressure, and is used to prevent flame out. The acceleration of the engine shafts serves as a proxy for Stall Margin (SM) since there is no on-board sensor for SM. The W_f signal that is ultimately provided to the fuel metering valve is the outcome of a selection process using a Min/Max approach[23]. The tail fan is similarly controlled with the PLA setting a commanded N_{fc}, where the controller sets a demanded torque from the electric motor, and the required limit logic can be simplified. Without a combustor, the high temperature safety requirements and engine blow out conditions are not applicable, leaving the main concern of fan rotational limits.

A block diagram of the set point controller is shown in Fig. 8, where the primary control loop is closed on N_f. The gains K_P and K_I of the PI controller are scheduled based on altitude, Mach number, and the power level (pwr)[16, 24–26]. This aids in producing a critically damped response at different power levels. The integrator term contains an integral anti-wind-up protection scheme[27] that includes the gain (IFB) as shown in Fig. 8. The output of the controller, W_f Reg, is the controller's desired fuel flow rate and W_f Cmd is the actual fuel flow rate after the Min/Max protection logic at the most recent step. For this study, the controller is designed to achieve the typical bandwidth of the fuel pump actuator of 6 Hertz (Hz) with a constraint of producing a gain margin of at least 6 dB and a phase margin greater than 60 degrees. This is achieved while maintaining a critically damped closed loop response. The protection logic is designed

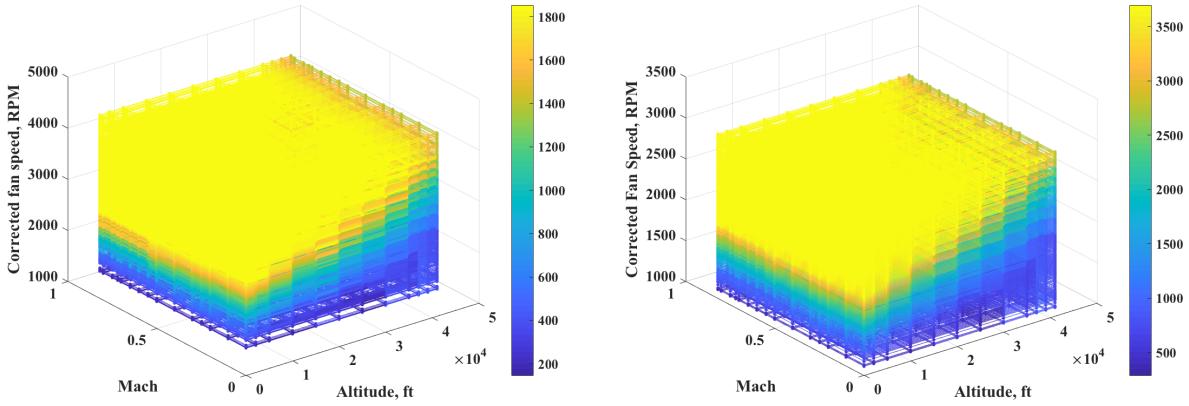

(a) Turbofan power extraction schedule.

(b) Tail fan power demand.

Fig. 7 The power schedules for the STARC-ABL model are shown as a function of Mach, altitude and corrected fan shaft speed in revolutions per minute (RPM). (a) The power extraction for one of the turbofans in horse power. (b) The power required by the tail fan.

to ensure that critical variables do not exceed their limits.

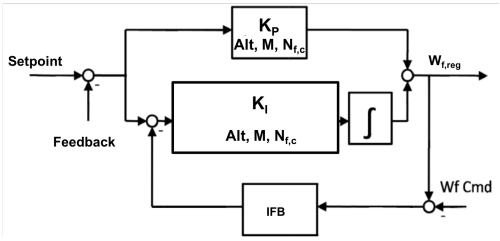

Fig. 8 Gain scheduled set point controller block diagram.

C. Electrical System Modeling

Two electrical power system models are used in this study that represent different levels of fidelity. The first one is a simple power flow model that is suitable to capture relevant electrical system effects, while focusing on the turbofan propulsion system response and stability across its operating envelope. The second one is a more detailed electrical power system model that can represent the specific electrical system component dynamics as well as the overall electrical power dynamics. The detailed electrical model is also better suited to capturing electrical faults and potential coupling between the turbomachinery and electrical systems. Though, given the relatively slow response of the propulsion system (a few Hz) and the fast response of the power system electronics (a few kilo-Hertz), there is not expected to be much dynamic interaction between the two systems, except in off-nominal operation or fault scenarios. However, it is important to note that the two subsystems (electrical and turbomachinery) are also controlled based on component controllers (engine control, motor control, generator control, etc.) working together.

1. Simple Electrical Power System Power Flow Modeling

The modeling technique used was based on power/load flow and is designed to provide a modular framework that includes buses, lines, and other electrical components that can be connected together to form the electrical distribution system. These general modeling techniques were created for use in system and control design studies. Power flow is a steady state method of modeling electrical systems. These models are based around lines linking different buses that are then relayed to generators or loads. The use of power flow provides a number of advantages: the overall system is

modular allowing for components to be added or removed easily; interaction with the model may come in the form of a specified power and/or current and voltage; components can be represented by equivalent circuits that match required fidelity; and simulation execution time is comparable to 0-D propulsion system modeling. Although these types of models come with many attractive attributes, they also require the major assumption that the system is in steady state. In this paper, this limitation is worked around by adding adjustment dynamics to take into account the shaft dynamics, which are generally the most influential contributor to the dynamics of the propulsion system. Additional dynamics that influence the applied shaft torque can then be introduced through the use of external transfer functions, which are empirically tuned to match the system. This combination of approaches results in a quasi-steady state modeling technique that can be used for steady state performance prediction and dynamic system responses. This dynamic behavior is limited to generalizations unless data can be found for model characterization. It should also be noted that this modeling technique was not developed for electrical subsystem control design as this would require a fully dynamic simulation of the electrical subsystem. The main governing equations that relate real and imaginary powers (P and Q respectively), added (via a generator, subscript G) or subtracted (via a load, subscript L) from the grid, to powers flowing between bus i and each neighboring bus j within the grid are shown in Eq. 2-3. Further details for the power flow approach in Chapman[28].

$$P_{Gi} = P_{Li} + \sum_{j=1}^{n} V_i V_j Y_{ij} cos(\delta_i - \delta_j - \gamma_{ij}) \tag{2}$$

$$Q_{Gi} = Q_{Li} + \sum_{j=1}^{n} V_i V_j Y_{ij} sin(\delta_i - \delta_j - \gamma_{ij}) \tag{3}$$

Table 2 Electrical component assumptions

Component	η
Generator	96%
Motor	96%
Inverter/Rectifier	98%
Cable	99.6%

Even with the power/load modeling approach taken here, the electrical system model is highly coupled. As a result, adjustments to this approach need to be made in order to address this coupling and create a modeling scheme that works with the T-MATS modular directional flow modeling technique. Creating this scheme begins with the realization that the nodal power is simply the product of the summation of each current entering the node and the nodal voltages. This insight leads to a modeling formulation where each line component obtains the upstream node voltage, then determines the downstream node voltage to determine the current, effectively removing the need for full system definition and allowing for modular components. For the model definition to work, a local solver must be introduced. For this work, a Newton-Raphson type solver (provided by T-MATS) was utilized. This localized solver determines a set of independent variables by monitoring and forcing dependent variables to be equal to zero. In this case, it is necessary that the number of independents match the number of dependents. The interfaces between the different models are handled by motor and generator models that translate shaft torque and speed into power. The electrical components used for this implementation are the generator, rectifier, DC bus, inverter, and motor. The electrical components are assumed to have the efficiencies shown in Table 2[13].

2. Detailed Electrical Power System Modeling and Control

The detailed electrical system model represents the STARC-ABL test article located at the NASA Electrified Aircraft Testbed (NEAT) facility at NASA's Plum Brook Station[29]. As such, this model represents the turbomachinery components (wing turbofan engines and tail fan) in the form of analogous electrical components to facilitate connecting them to the electrical power system. Since this model represents the current architecture at NEAT, the power requirements are less than those of the proposed STARC-ABL architecture from Section III. In addition, the modeling of the electrical components is based on the existing hardware and test specifications at the NEAT facility. So, while the detailed electrical model does have more fidelity, it is also constrained by its intended purpose to model the test article.

The detailed electrical system model shown in Fig. 9 was created in MATLAB/Simulink with the SimPowerSystems toolbox©. SimPowerSystems is a library of power system components that includes fundamental electrical elements, power electronic devices, and electrical machines and drives that are used to construct models for execution in the Simscape environment. In a Simscape model, flow of electric power is represented by connections between components,

as in a circuit diagram; the state of the system (voltages and currents) can be measured at any point along these physical connections. Typical Simulink connections are reserved for non-electrical signals, which include gate signals and controls. The Simulink block diagram interface allows the user to easily and quickly implement changes or additions to the system.

The majority of the high power electronics are represented by using components in the SimPowerSystems toolbox, where the component parameters are defined from vendor data or similar hardware information. Some components from the representative STARC-ABL test article are not included in the detailed electrical model since they are related to the facility setup. The primary electrical component in the detailed model is the motor model, which is represented using the permanent magnet synchronous motor block from the SimPowerSystems library. Specific input parameters are typically defined by vendor data and include stator phase resistance, armature inductances, motor constant, rotor inertia, rotor viscous damping, number of pole pairs, and rotor Coulomb friction. In addition, the back Electro-Motive Force (EMF) waveform has been specified as sinusoidal and the rotor type as salient-pole. This is just one example of the modeling fidelity that is used within the Simscape model and how it differs when compared to the power flow components used within the T-MATS model.

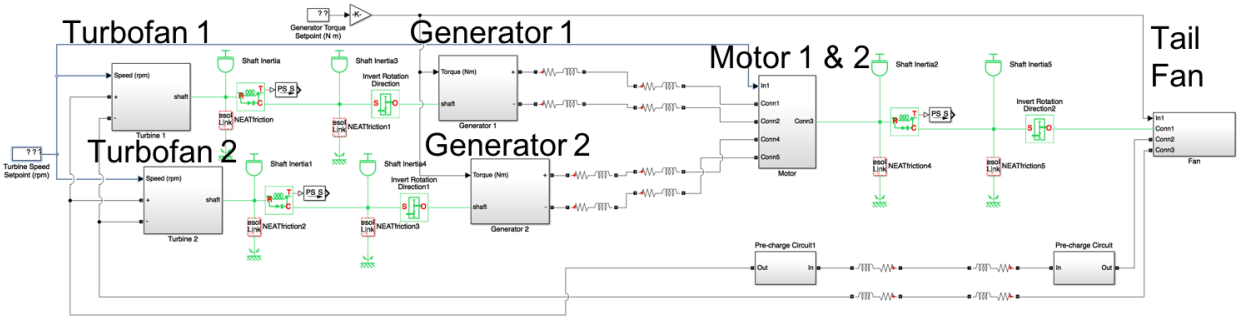

Fig. 9 Top level MATLAB/Simulink diagram of electrical power system using components from the Simscape toolbox.

The electrical controller subsystem in the generator block contains all inverter command signals. The torque command uses speed feedback from the driving motor to calculate a torque based on a function of the speed squared. The controls are made up of a PI speed controller (or torque controller) and a vector controller that sends Pulse Width Modulation (PWM) signals to the inverter. The speed controller is a SimPowerSystems library block, and the vector controller was modified from a library block to include field oriented control and flux weakening control. Inverter input parameters include DC link capacitance, insulated gate bipolar transistor (IGBT) and diode forward voltages, and IGBT shutoff time constants. Speed control input parameters include the speed reference acceleration limits, PI gains, speed measurement low-pass filter cutoff frequency, and the torque reference output limit. Field oriented control input parameters include the inverter switching frequency, integral gain for the flux weakening control, and proportional-integral-derivative gains for the current controllers. A number of motor parameters are fed back into the inverters, including the direct and quadrature stator voltages, rotor position, and rotor speed.

The Simscape electrical power system model is set up for a very specific purpose that primarily includes testing at the NEAT facility, where the electrical components are configured at a lower power level. Integration with the T-MATS propulsion system proved to be a challenge, primarily due to the different power levels and simulation requirements between the two models. Simply replacing the emulated propulsion elements in the Simscape model with T-MATS propulsion models was not feasible. Instead, the effects of the T-MATS propulsion system components were integrated in an open loop manner by incorporating the required inputs to the Simscape model (for example: the LPC speeds from the wing turbofan engines and the tail fan speed). This type of integration allows comparisons between the simple and detailed electrical models. In addition, the efficiencies of the Simscape power components used in the detailed electrical model must also be taken into account when comparing the two electrical models. The efficiency of the motor is dependent on the torque input, so the scaling was performed such that the torque values were within the same range for the example scenarios used.

V. Results

This section contains the results of the closed loop dynamic propulsion system model integrated with the simple electrical system model. First, propulsion system control considerations will be illustrated for the control design across all flight conditions on the PWLM, followed by the control system performance applied to the integrated nonlinear T-MATS model. The more detailed electrical system model is used with propulsion system data to investigate the accuracy of the simple power flow electrical model integrated with T-MATS. Finally, efficiency improvements about the cruise condition are investigated with ensured stable operation throughout the flight envelope.

A. Linear Propulsion System Simulation

The T-MATS PWLM model is simulated at 726 operating points throughout the flight envelope to explore the controlled rise time response of the turbofan engine (the time required for the fan speed to increase from 10% to 90% of the change in response to a step command), where a step command of 10% is applied to the PLA for all conditions. However, it should be noted that a maximum of 80^o PLA is enforced. A similar response investigation is done for the tail fan. It was found that the electric motor driving the tail fan enables a shorter rise time when compared to the turbofan driven by a combustion process as was expected. Thus, it is not shown here. Dynamic response times are shown as a histogram in Fig. 10(a), where most of the transient responses of the engine are within three seconds and all of them are within five seconds.

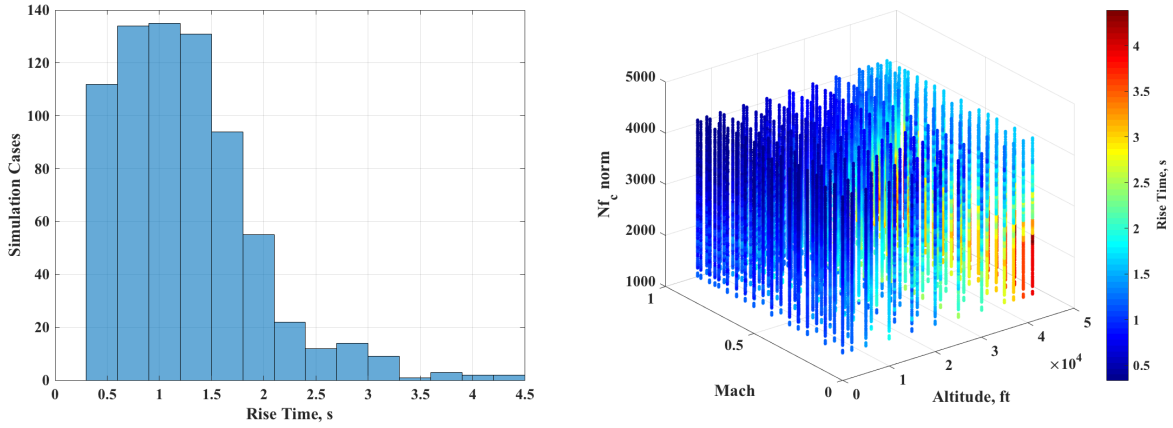

(a) Rise time histogram.

(b) Rise time across flight condition.

Fig. 10 (a) Rise time of turbofan simulation at each flight condition linear design point. (b) Rise time changes with respect to the Mach, altitude, and corrected fan speed.

The rise time is shown as a color coded plot across the flight envelope with respect to Mach, altitude, and corrected fan speed in Fig. 10(b). The blue represents a shorter rise time and the red a longer rise time. An interesting feature here is that, typically, a traditional turbofan response is the longest at idle (or low corrected fan speeds) and faster at higher power settings. This is due to the need to overcome the large inertias. This did not appear to be the case for the STARC-ABL configuration. Here the longer response times of the engine are shown to be at higher altitudes where the power being extracted from the engine is a larger percent of available power.

In addition to providing acceptable rise time, the turbofan controller must be able to operate throughout the flight envelope without encountering a stall event that results in a rapid loss of thrust. While running the rise time investigation, the resulting minimum HPC SM was obtained for each case and is shown as a histogram in Fig. 11. In the vast majority of cases, there is adequate stall margin; however, in approximately five cases the stall margin does go below the 10% threshold. This indicates that there needs to be some fine tuning of the limiter to ensure operability throughout all flight conditions when applied to the nonlinear T-MATS model.

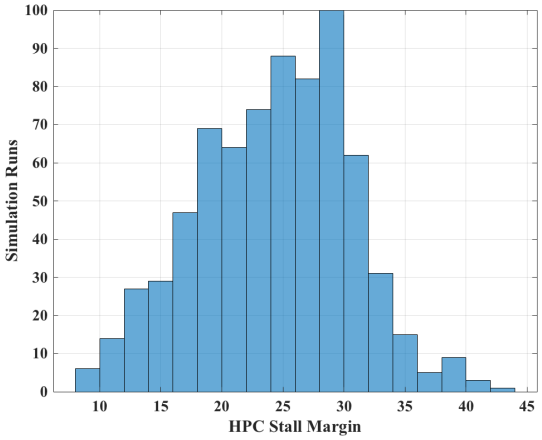

Fig. 11 Histogram of minimum HPC stall margin due to transient responses to steps of 10% of PLA across the operating flight envelope.

B. Integrated Propulsion System Model at Takeoff

The main transient requirement of the propulsion system is defined by the Federal Aviation Administration (FAA)[30], where the thrust must increase from flight idle to 95% rated takeoff power within five seconds.

1. STARC-ABL model with T-MATS turbomachinery components and Power Flow electrical system components

The control response of the STARC-ABL integrated model is investigated for a new and deteriorated propulsion system to determine the thrust and power that needs to be provided to the tail fan in order to meet the FAA thrust requirement. The simulation is started at zero altitude and Mach number at a PLA setting of 51^o to simulate the flight idle condition. The PLA step transient to a maximum of value of 80^o is then applied at the one second mark. The PLA provides an N_{fc} command to each geared turbofan (shown as a dashed red line in Fig. 12(a)) and tail fan (dashed magenta line). The controller response is shown for a new engine (GTF1 solid blue), an end of life engine (GTF2 dashed blue), and the tail fan (solid black new and dashed black end of life). For the end of life engine response there is a slight offset in N_{fc} due to the initial limiter design of the maximum exhaust gas temperature (EGT) being triggered in the protection logic. The limit was set from the maximum value of all of the flight conditions based on a new engine. When the engine deteriorates, the maximum value is exceeded during larger transient maneuvers and high power settings. This limit was adjusted for the flight mission profile studies that follow by raising the EGT limit value by 5%. As was noted before, the deterioration has less of an impact on the bypass flow, this results in the tail fan response being very similar throughout its life cycle.

The net thrust response of a new (GTF1) and end of life (GTF2) geared turbofan is able to meet the FAA transient requirement as shown in Fig. 12(a). The shaded green area is the amount of time that the thrust has to meet the required 95% maximum value threshold. Both the new and deteriorated results for the geared turbofans and tail fan are able to meet the requirement in less than 3 seconds shown in Fig. 12(a). The new turbofan engine is able to respond about a half second faster than the deteriorated engine.

One of the critical operability considerations of the geared turbofans is the available SM, shown for the LPC and HPC in Fig. 12(b). The limiter was designed to provide a margin of at least 10% for both the HPC and LPC. One of the stability concerns for the STARC-ABL was the low LPC SM at idle conditions. It is shown in Fig. 12(b) that the HPC has plenty of margin throughout the transient maneuver; however the LPC starts near the limit threshold and violates the limit during the initial transient. While the transient starts near the limit threshold, initial expectations of the LPC SM response was for the positive PLA transient to cause an increase in the LPC stall margin. Although, that eventually holds true with the STARC-ABL vehicle, the LPC SM initially responds in an inverse relationship to the PLA, which caused a violation of the limit. To improve the transient response for the following mission profile study, the VBV schedule was altered to have the valve open by 10% during idle conditions to improve the LPC SM.

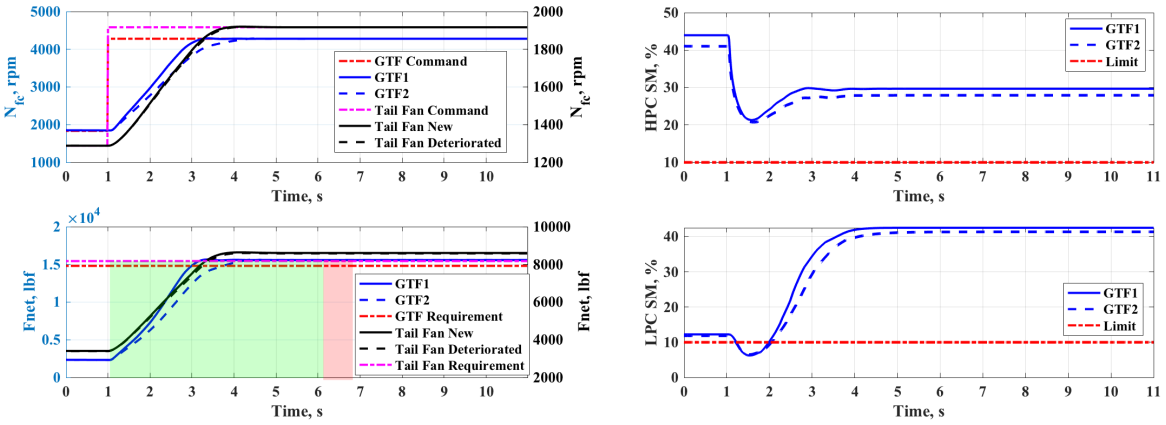

(a) Corrected fan speed controller and resulting thrust response.

(b) Stall margin for the HPC and LPC.

Fig. 12 FAA transient response for GTF1 (new engine) and GTF2 (end of life engine), and tail fan.

2. Power System Modeling Comparison

Results from integrating the detailed electrical power system model via inputs from the T-MATS propulsion component models are shown in Fig. 13 for the relevant parameters of the power system as it is connected to the propulsion system elements. These include the turbofan engine power extracted by the generator, the tail fan required power, and power provided to a given motor that drives the tail fan. These results, based on the takeoff profile, are compared with those from the simple model. Specific parameters in the detailed power system, such as the input-output dynamics of the controllers, are not included here since the primary interest is comparing results with the simple power flow model, which does not have similar parameters.

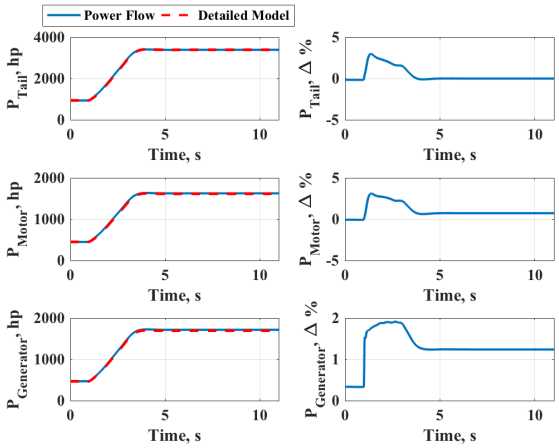

Fig. 13 Power system modeling comparison for FAA transient, illustrating percent differences between power flow and more detailed Simscape approaches.

The takeoff profile is defined with the altitude and Mach number set to zero. The PLA input is varied from 51 to 80 in 0.015 seconds. The LPC speed was applied directly to the generator. Output results comparing the simple and detailed electrical models are shown in Fig. 13, where they are in good agreement. The largest percent differences are in the transient as expected, but are generally less than 3%, while in steady state operation, the models agree within about 1%. For large system trade studies, the power flow modeling approach should provide an adequate level of fidelity.

Further evaluation with the more detailed model can be explored in future studies investigating fault conditions.

C. Investigation to Improve Efficiency by Modifying the Power Management

An investigation of the assumed NPSS power split from the geared turbofans to the tail fan is conducted about the cruise conditions shown in Fig. 5. The goal of the investigation is to find the optimal power required by the tail fan to provide a minimum thrust specific fuel consumption (TSFC). The baseline NPSS model's power split was not explicitly designed throughout the flight envelope. Rather, the power split is a consequence of the way the tail fan motor shaft power is controlled by the NPSS solver. Specifically, the motor power is set to 3500 hp, with a constraint that limits this motor power such that the ratio of generator power extraction to total power added to the LP shaft by the LPT does not exceed 33%, which is the ratio that the engine runs at the top-of-climb design point. This concept of operation for the power split was chosen as a simple but suboptimal way to ensure that the generator does not compromise turbomachinery operability. Note that the percent changes in TSFC and other variables, found in this investigation, are changes relative to this initial design approach. At every cruise condition, defined by a specific Mach number and altitude combination, a PLA sweep was conducted for the NPSS design model. The minimum TSFC in the PLA sweep at a given cruise condition set the baseline from which this study does a comparison. The results from a search for an improved TSFC are shown in Fig. 14(a) at an altitude of 35,000 ft and for a Mach number of 0.75 (blue) and 0.8 (red). The baseline that serves as a point of comparison is denoted by a large 'X' for each Mach number. While the other cruise conditions shown in Fig. 5 do vary slightly, the condition shown is representative of the trends found.

To conduct the search for a potential change in the energy split between the geared turbofan and the tail fan the following procedure was followed:

1) The STARC-ABL vehicle was simulated at the desired operating condition.
2) The tail fan PLA was then swept in step increments from idle to maximum power.
3) At each step change in the tail fan PLA, the geared turbofan PLA was adjusted such that the net thrust obtained from summing the two geared turbofans and the tail fan equaled that of the baseline operating condition.
4) The TSFC was then calculated by summing the fuel flow rate of the two geared turbofans and dividing by the overall vehicle net thrust.

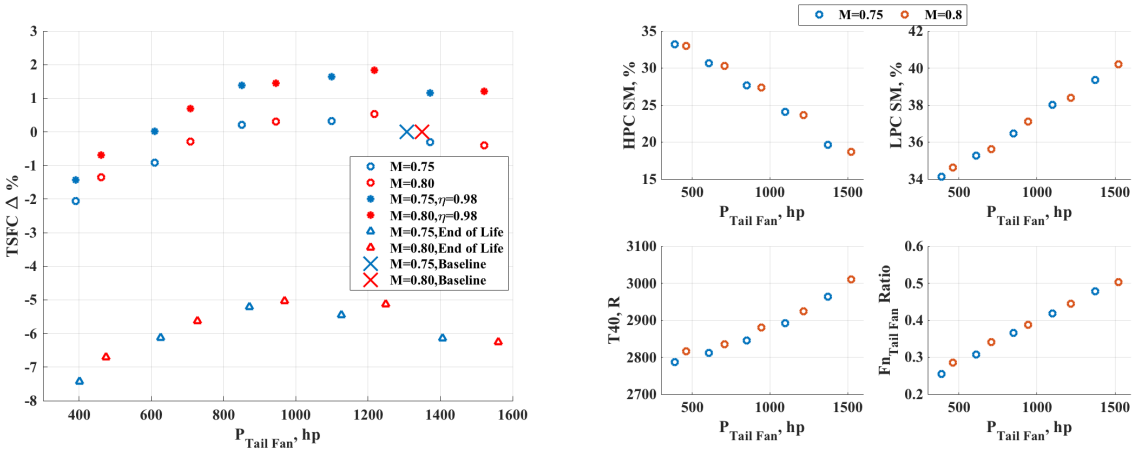

(a) Change in TSFC versus tail fan power required from one turbofan.

(b) Impacts on HPC Stall margin, LPC Stall Margin, combustor exhaust temperature, and thrust ratio.

Fig. 14 Investigation of tail fan power on TSFC and propulsion stability parameters. Note that a positive change indicates an improvement.

The percent change in the obtained TSFC is then shown in Fig. 14(a), where a positive percent change indicates an improved TSFC over the baseline schedule. The power required along the x-axis of Fig. 14(a) is from one of the motors driving the tail fan, thus multiplying by two would give the overall system power. Results show that there is, in general, a desirable split between the tail fan power required and the TSFC, where either too little power or too much power will reduce TSFC. The nominal STARC-ABL configuration denoted with 'o' symbols in the plot have the potential for

approximately 0.5% TSFC improvement over the NPSS design schedule at these cruise conditions. This benefit can be realized with a simple schedule change, if approximately 200 hp less is delivered to the tail fan from each turbofan and slightly more of the overall net thrust is generated by the geared turbofans.

The same analysis that was conducted for the nominal design was conducted for two other cases where the vehicle is at an end of life condition (denoted by triangles) and an improved motor/generator efficiency from 0.96% to 0.98% (denoted by solid multipoint stars). The end of life engine model is obtained by changing flow capacity scalars and efficiencies for all of the turbomachinery components in the model. The general trend of the curves is maintained for these conditions. An improvement in the electrical system performance provides nearly an equivalent TSFC improvement of almost 2%, whereas a deteriorated system can expect to have nearly a 5% penalty in TSFC.

Operability impacts of changing the energy split between the geared turbofan and the tail fan are shown in Fig. 14(b) for the nominal case. In general, a linear relationship between the power required by the tail fan and key parameters of interest is established. As expected, the less power extracted from the turbofan to drive the tail fan, the more operability margin for HPC SM and combustor exit temperature, $T40$. The LPC SM is improved with more power extraction; however, at cruise, where TSFC improvements can have the most impact, the LPC SM is sufficient to not be a concern.

D. Integrated Propulsion System with Simple Electrical Components for Full Flight Envelope

A 900 nmi mission profile shown in Fig. 15 is used to ensure operability of the STARC-ABL vehicle. To investigate the operability of the vehicle, the STARC-ABL is simulated over a range of conditions: a healthy condition denoted as nominal, an end of life condition that has deteriorated performance, and an optimized schedule that uses the change in power split between the geared turbofans and tail fan, as suggested in the previous section to improve the TSFC. The change in the power split occurs at the cruise point of approximately 50 min.

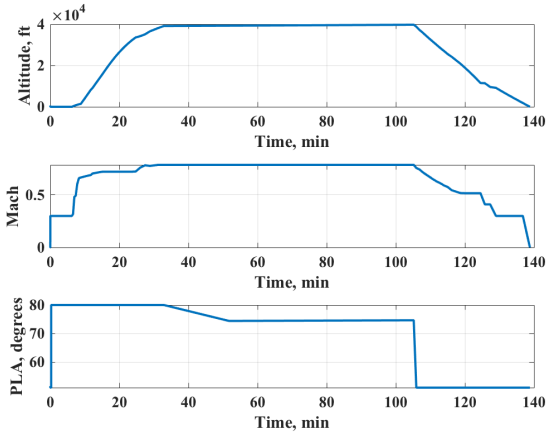

Fig. 15 Expected future 900 nmi mission profile for large single aisle class vehicles.

The key operability parameters for the STARC-ABL vehicle across the mission profile are shown in Fig. 16. For the given mission profile, a simple gain scheduled full flight envelope controller and limit logic is able to ensure safe operation of the vehicle for all three of the aforementioned cases: nominal, deteriorated, and optimized. For each parameter, the percent differences between nominal and each of the two cases are also shown in the right column of plots in Fig. 16. The limit that is of most concern currently is the LPC SM near idle conditions, which characterize the ground taxi and landing portions of the flight profile. This could be a result of the more conservative calculation of the LPC SM used in this study at low spool speed conditions, and needs to be explored further. As discussed previously in Section V, a slight modification of the bleed schedule can be introduced to help ensure that LPC SM is no longer violated. The EGT temperature limit was nearly violated during the rapid takeoff acceleration, particularly for the deteriorated engine, but then benign for the rest of the flight mission.

During the mission profile, the power split schedule is modified to accommodate the TSFC study by reducing the PLA to the tail fan by two degrees and increasing the PLA to the geared turbofans by two degrees. This results in an average reduction in TSFC during the cruise phase of 0.58% (at approximately the 50 min mark on the timeline) similar

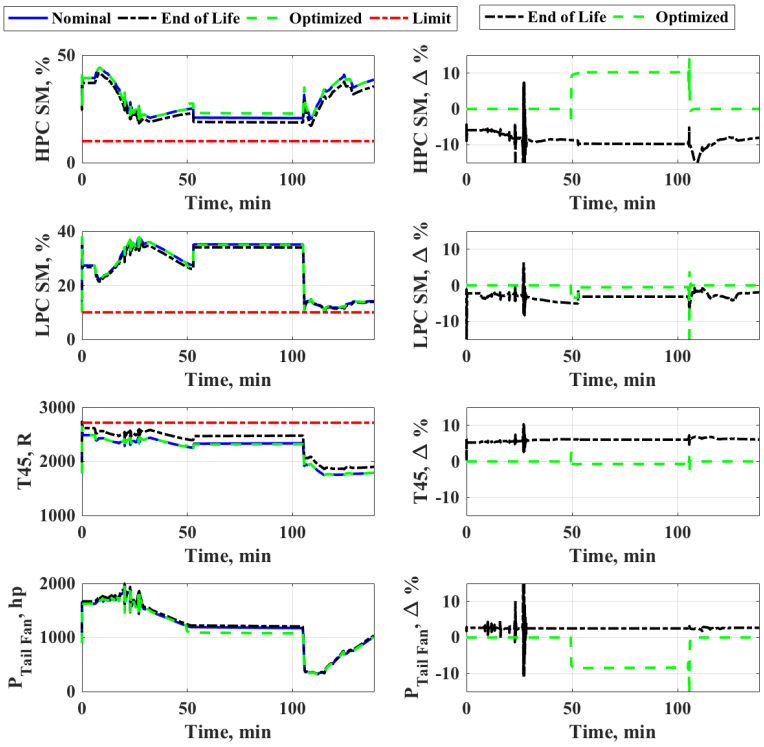

Fig. 16 Operability investigation of STARC-ABL over 900 nmi mission profile.

to that obtained in the previous section. Deterioration of the vehicle had the greatest impact on the HPC SM, where there is an average decrease of 8.2%. The deteriorated propulsion system also requires more power to be extracted by an average of 2.6%, as opposed to the optimized schedule having an average reduction at the cruise point of 8.5%.

VI. Conclusion

A nonlinear dynamic model with full flight envelope controller was developed and shown to operate stably while meeting performance metrics for a turbofan engine with a large percentage of power extraction, suitable for a single aisle aircraft with a tail fan for boundary layer ingestion. An electrical system model using a simple power flow approach was integrated into existing modeling tools used for dynamic simulation of the turbomachinery of the vehicle. In addition to the simple power flow model of the electrical system, a more detailed model was used for comparison at a key vehicle transient flight condition. For large system trade studies, the power flow modeling approach should provide an adequate level of fidelity. The more detailed model can be used in future studies to investigate fault conditions. An exploration of potential improvements in efficiency for the vehicle was conducted by adjusting the power split between the turbofans and tail fan. It was shown through simple adjustments in the power schedule that the thrust specific fuel consumption can be reduced by a little over 0.5% at cruise. Finally, an operability study of the vehicle was conducted using a 900 nmi mission profile for a nominal vehicle configuration, a deteriorated vehicle at the end of its operating life, and an optimized power schedule to improve efficiency. All of the configurations were able to fly the mission profile avoiding any stability issues. One important feature that is illustrated in the deteriorated engine, is that the core of the engine is impacted more than the bypass. This could imply that as the turbomachinery components degrade it may be beneficial to generate more thrust from the tail fan.

VII. Acknowledgments

The authors would like to thank the Hybrid Gas-Turbine Electric Propulsion subproject of the Advanced Air Transport Technology project under the NASA Aeronautics Mission Directorate's Advanced Air Vehicles program for their support of this work, and James Felder for providing valuable insight and the steady state propulsion system design model.

References

[1] J. Shin, "NASA Aeronautics: Strategic Implementation Plan," NASA NP-2017-01-2352-HQ, 2017. doi:10.1057/9781137294678.0652.

[2] Thole, K. A., and Whitlow Jr., W., *Commercial Aircraft Propulsion and Energy Systems Research: Reducing Global Carbon Emissions*, The National Academies of Science Engineering Medicine, 2016. doi:10.17226/23490.

[3] Papathakis, K. V., Kloesel, K. J., Lin, Y., Clarke, S. C., Ediger, J. J., and Ginn, S. R., "NASA Turbo-electric Distributed Propulsion Bench," *52nd AIAA/SAE/ASEE Joint Propulsion Conference*, AIAA 2016-4611, 2016, pp. 1–17. doi:10.2514/6.2016-4611.

[4] Mikic, G. V., "Design Studies of Thin-Haul Commuter Aircraft with Distributed Electric Propulsion," *16th AIAA Aviation Technology, Integration, and Operations Conference*, AIAA 2016-3765, 2016. doi:10.2514/6.2016-3765.

[5] Lents, C. E., Hardin, L. W., Rheaume, J., and Kohlman, L., "Parallel Hybrid Gas-Electric Geared Turbofan Engine Conceptual Design and Benefits Analysis," AIAA 2016-4610, 2016. doi:doi:10.2514/6.2016-4610.

[6] Seitz, A., Isikveren, A. T., and Hornung, M., "Pre-Concept Performance Investigation of Electrically Powered Aero-Propulsion Systems," *49th AIAA/ASME/SAE/ASEE Joint Propulsion Conference*, AIAA 2013-3608, 2013, pp. 1–16. doi:10.2514/6.2013-3608.

[7] Moore, M. D., and Fredricks, B., "Misconceptions of Electric Aircraft and their Emergent Aviation Markets," *52nd Aerospace Sciences Meeting*, AIAA 2014-0535, 2014. doi:10.2514/6.2014-0535.

[8] Pornet, C., Gologan, C., Vratny, P. C., Seitz, A., Schmitz, O., Isikveren, A. T., and Hornung, M., "Methodology for Sizing and Performance Assessment of Hybrid Energy Aircraft," *Journal of Aircraft*, Vol. 52, No. 1, 2015, pp. 341–352. doi:10.2514/1.C032716.

[9] Seok, J., Kolmanovsky, I., and Girard, A., "Integrated / Coordinated Control of Aircraft Gas Turbine Engine and Electrical Power System : Towards Large Electrical Load Handling," *IEEE Conference on Decision and Control*, 2016, pp. 3183–3189.

[10] Seitz, A., Schmitz, O., Isikveren, A. T., and Hornung, M., "Electrically Powered Propulsion: Comparison and Contrast to Gas Turbines," *Deutscher Luft- und Raumfahrtkongress*, 281358, 2012, pp. 1–14.

[11] Jansen, R., Brown, G. V., Felder, J. L., and Duffy, K. P., "Turboelectric Aircraft Drive Key Performance Parameters and Functional Requirements," *51st AIAA/SAE/ASEE Joint Propulsion Conference*, AIAA 2015-3890, 2015, pp. 1–10. doi:10.2514/6.2015-3890.

[12] Green, M., Schiltgen, B., and Gibson, A., "Analysis of a Distributed Hybrid Propulsion System with Conventional Electric Machines," *48th AIAA/ASME/SAE/ASEE Joint Propulsion Conference & Exhibit*, AIAA-2012-3768, 2012, pp. 1–12. doi:10.2514/6.2012-3768.

[13] Welstead, J., and Felder, J. L., "Conceptual Design of a Single-Aisle Turboelectric Commercial Transport with Fuselage Boundary Layer Ingestion," *54th AIAA Aerospace Sciences Meeting*, AIAA-2016-1027, 2016, pp. 1–17. doi:10.2514/6.2016-1027.

[14] Lytle, J. K., "The Numerical Propulsion System Simulation: A Multidisciplinary Design System for Aerospace Vehicles," NASA/TM 1999-209194, 1999.

[15] Chapman, J. T., Lavelle, T. M., May, R. D., Litt, J. S., and Guo, T., "Propulsion System Simulation Using the Toolbox for the Modeling and Analysis of Thermodynamic Systems (T-MATS)," NASA TM 2014-218410, Nov. 2014.

[16] Lawrence, D. A., and Rugh, W. J., "Gain Scheduling Dynamic Linear Controllers for a Nonlinear Plant," *Automatica*, Vol. 31, No. 3, 1995, pp. 381–390.

[17] Spang, H. A., and Brown, H., "Control of Jet Engines," *Control Engineering Practice*, Vol. 7, No. 9, 1999, pp. 1043–1059. doi:10.1016/S0967-0661(99)00078-7.

[18] Chen, C., Sui, Y., Zhao, J., and Zhao, J., "Coordinated Switching Control of Thrust Tracking and Safety Protection for Aero-Engines," *Proceedings of the 33rd Chinese Control Conference*, IEEE 2014-6895616, 2014, pp. 4050–4055. doi: 10.1109/ChiCC.2014.6895616.

[19] Du, X., Richter, H., and Guo, Y. Q., "Multivariable Sliding-Mode Strategy with Output Constraints for Aeroengine Propulsion Control," *Journal of Guidance, Control, and Dynamics*, Vol. 39, No. 7, 2016, pp. 1631–1642.

[20] Xiaofeng, L., Shi, J., Yuan, Y., and An, S., "Multiobjective Control System Controllers Design Based on Switching and Applications," *IEEE Aerospace and Electronic Systems Magazine*, Vol. 30, No. 1, 2015, pp. 32–42.

[21] Zheng, Q., and Zhang, H., "A Global Optimization Control for Turbofan Engine Acceleration Schedule Design," *Proceedings of the Institution of Mechanical Engineers: Journal of Aerospace Engineering*, Vol. 232, No. 2, 2016.

[22] Liu, X., and An, S., "Smooth Switching Controller Design for Multiobjective Control Systems and Applications," *Journal of Aerospace Engineering*, Vol. 29, No. 4, 2016.

[23] May, R., Csank, J., Litt, J. S., and Guo, T., "Commercial Modular Aero-Propulsion System Simulation 40K," NASA/TM 2010-216810, 2009.

[24] Csank, J., Ryan, M., Litt, J. S., and Guo, T.-H., "Control Design for a Generic Commercial Aircraft Engine," *46th Joint Propulsion Conference and Exhibit cosponsored by the AIAA, ASME, SAE, ASEE*, AIAA 2010-6629, 2010, pp. 1–14. doi:10.2514/6.2010-6629.

[25] Pakmehr, M., Fritzgerald, N., Feron, E. M., Shamma, J. S., and Behbahani, A., "Gain Scheduling Control of Gas Turbine Engines: Stability by Computing a Single Quadratic Lyapunov Function," GT2013-96012, Jun. 2013.

[26] Rugh, W. J., "Analytical Framework for Gain Scheduling," *IEEE Control Systems Magazine*, Vol. 11, 1991, pp. 74–84.

[27] Martin, S., Wallace, I., and Bates, D. G., "Development and Validation of a Civil Aircraft Engine Simulation Model for Advanced Controller Design," *Journal of Engineering for Gas Turbines and Power*, Vol. 130, No. 5, 2008.

[28] Chapman, J. W., and Litt, J. S., "An Approach for Utilizing Power Flow Modeling in Hybrid Electric Propulsion Systems," *AIAA Propulsion and Energy Forum*, AIAA - To Be Published, 2018.

[29] Dyson, R. W., "NASA Electric Aircraft Test Bed (NEAT) Development Plan - Design, Fabrication, Installation," NASA TM 2016-219085, 2016.

[30] Federal Aviation Administration, "Title 14 Part 33.73 Power or Thrust Response," Federal Aviation Regulation (FAR), 2018.

VIII. Appendix

For a closer look of the specific engine station performance, the cruise condition steady state matching of P_T, T_T, and W can be seen in Fig. A.1. The matching across all of the turbomahcinery flow stations never exceeds a half a percent difference at cruise. The average steady state matching of the tail fan and impacts of the deterioration can be seen in Table A.1. Similar percent differences are obtained compared to the geared turbofan with the exception of a slightly larger error in the mass flow due to the changes in the VAFN schedule. The main takeaway is that the deterioration for the tail fan has a negligible impact.

Table A.1 T-MATS Tail Fan % Variation from NPSS

	Averaged Stations		
	W	P_T	T_T
New	2.62	0.67	0.11
End of Life	2.41	0.64	0.09

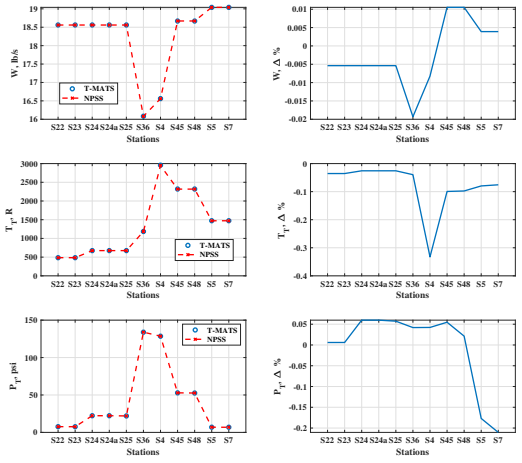

(a) Turbofan Core Stations.

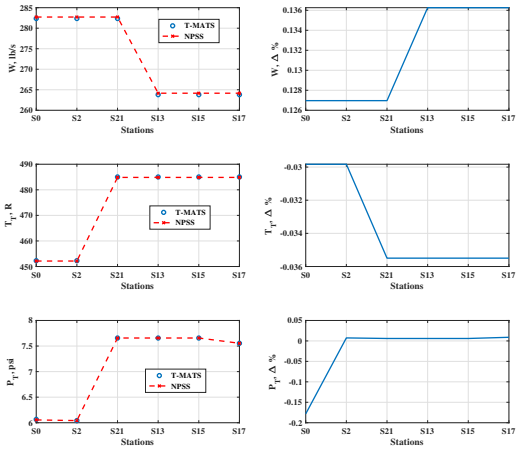

(b) Turbofan Bypass Stations.

Fig. A.1 Steady state cruise condition matching of T-MATS control model to NPSS design model.